Inorganic Chemistry

Article

pubs.acs.org/IC

Understanding Intrinsic Light Absorption Properties of UiO-66 Frameworks: A Combined Theoretical and Experimental Study

Kevin Hendrickx,[†,‡] Danny E. P. Vanpoucke,[‡] Karen Leus,[†] Kurt Lejaeghere,[‡] Andy Van Yperen-De Deyne,[‡,§] Veronique Van Speybroeck,[*,‡] Pascal Van Der Voort,[*,†] and Karen Hemelsoet[*,‡]

[†]Department of Inorganic and Physical Chemistry, Center for Ordered Materials, Organometallics and Catalysis (COMOC), Ghent University, Krijgslaan 281 (S3), 9000 Ghent, Belgium

[‡]Center for Molecular Modeling (CMM), Ghent University, Technologiepark 903, 9052 Zwijnaarde, Belgium

Supporting Information

ABSTRACT: A combined theoretical and experimental study is performed in order to elucidate the effects of linker functional groups on the photoabsorption properties of UiO-66-X materials. This study, in which both mono- and difunctionalized linkers (with X = OH, NH_2, or SH) are investigated, aims to obtain a more complete picture of the choice of functionalization. Static time-dependent density functional theory calculations combined with molecular dynamics simulations are performed on the linkers, and the results are compared to experimental UV/vis spectra in order to understand the electronic effects governing the absorption spectra. The disubstituted linkers show larger shifts than the monosubstituted variants, making them promising candidates for further study as photocatalysts. Next, the interaction between the linker and the inorganic part of the framework is theoretically investigated using a cluster model. The proposed ligand-to-metal-charge transfer is theoretically observed and is influenced by the differences in functionalization. Finally, the computed electronic properties of the periodic UiO-66 materials reveal that the band gap can be altered by linker functionalization and ranges from 4.0 down to 2.2 eV. Study of the periodic density of states allows the band gap modulations of the framework to be explained in terms of a functionalization-induced band in the band gap of the original UiO-66 host.

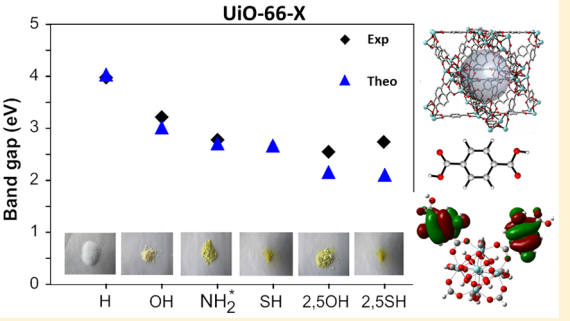

1. INTRODUCTION

Metal−organic frameworks (MOFs) are a versatile class of crystalline porous materials constructed from inorganic clusters that are linked by organic moieties. Thanks to the large number of different building blocks available, MOFs have a high level of tunability, which has led to considerable research interest in the fields of catalysis, gas storage, chemical sensing, and separation.[1−3] Recent developments in the field have extended the research domain of MOFs toward light-based applications, more specifically their use in photocatalysis[4,5] and as luminescent materials,[6] where the tunability of the frameworks appears to be a great asset. The luminescence properties of MOFs have been shown to be very unique,[7] since luminescence can originate from both the metal centers and the organic linkers as well as via charge transfer between them or between a guest species and the framework.[4,6] Ideally, this allows for exact tuning of the framework for a specific application and opens possibilities toward, e.g., biomedical applications,[8] light-emitting diode devices,[9] and chemical sensors.[10]

Classical photocatalysis originated in the 1970s, when Fujishima and Honda presented their method for the photolysis of water.[11] Since then, researchers have concentrated mainly on chalcogenide semiconductors, such as metal oxides (TiO_2, ZnO, and ZrO_2), sulfides (e.g., CdS, ZnS, etc.), or combined systems.[12−18] The classic photocatalysts suffer from two major limitations that hamper their use in renewable and clean processes and materials: (1) the activity and availability of the active sites is insufficient, and (2) the materials lack activity in the visible range of the spectrum. Recent efforts to overcome these hurdles have led to the synthesis of a whole series of new materials including dye-sensitized systems,[19] doped metal chalcogenides,[20,21] nanomaterials,[22] and also MOFs.[4] Since MOFs are built out of small nanoclusters and aromatic ligands, they offer strong possibilities to remedy the limitations of the classic photocatalysts. The organization of molecular building units into one crystalline material, combined with a high surface area, makes it possible to engineer the materials toward specific applications.[23,24] MOFs are used as photocatalysts following two different routes: the MOF framework acts as an antenna and therefore (1) the material itself has unsaturated open metal sites as catalytic sites or (2) the energy is transferred to incorporated guest species.[4] The use of MOFs as photocatalyst has proven to be very successful, notably in chiral synthesis,[25]

Received: July 17, 2015

DOI: 10.1021/acs.inorgchem.5b01593
Inorg. Chem. XXXX, XXX, XXX−XXX

CO_2 reduction,[26] hydrogen production,[27] and organic synthesis.[28,29] In spite of this growing research interest, this research area is still an emerging field, and important issues such as activity, efficiency and stability require more in-depth studies.[30]

Herein we focus on the series of UiO-66 materials,[31] which contain Zr−O corners and benzene-1,4-dicarboxylate (BDC) linkers. The structure of the framework and the different building units are shown in Figure 1. These materials are

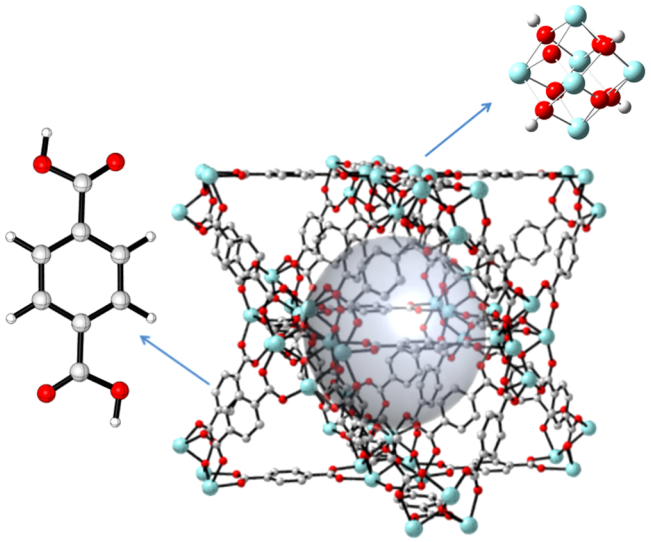

Figure 1. Structure of the UiO-66 framework, in which an inorganic $Zr_6O_4(OH)_4$ unit and an organic H_2BDC linker (which is first deprotonated to give BDC^{2-}) coordinate to form a porous structure. The gray volume represents the porous cage formed in the three-dimensional material. Atoms are colored as follows: C, gray; O, red; H, white; Zr, light blue.

known to be very stable and have been intensively studied for a whole range of applications.[32−37] Exploration of the UiO-66 materials for light-harvesting and photocatalytic applications started with Garcia and co-workers,[38] who studied hydrogen generation using the amino-functionalized material. They showed that the NH_2 group causes a shift in the absorption spectrum toward the visible range, which was afterward applied to Cr(VI) reduction and oxidation of alcohols,[39] a series of aerobic organic transformations,[40] and CO_2 reduction[41] by other groups. The latter study also provided the first experimental insight into the mechanism and processes that occur during irradiation of UiO-66 and gave the first evidence for charge transfer from the linker toward the Zr corners. Shen et al.[42] studied the electronic effect of ligand substituents on the photocatalytic activity of the UiO-66 framework and found that the corresponding rates are linearly correlated with their Hammett coefficients. They proposed that the functional groups would promote charge transport and separation of the carriers in the framework. The use of a mixed-linker approach has recently been reported to improve the performance in the photocatalytic oxidation of alcohols.[43] Recent studies of the periodic UiO materials confirmed the experimental band gap modulations via calculations based on density functional theory (DFT). Flage-Larsen and co-workers[44] employed both semi-local and hybrid functionals to model the band gap modulation of the parent UiO-66 material and its NO_2 and NH_2 linker-substituted variants. The resulting band gap reduction could be explained on the basis of lone-pair interactions with the bulk material. Very recently, Musho et al.[45] examined the same set of materials, and the band gap modulation could be explained on the basis of the projected density of states of the periodic materials and excited-state simulations of the linker components. Similar studies of the Ti-MIL-125 MOF showing the possibilities of this engineering approach have been reported by Hendon and co-workers.[46] The term "band gap" is employed these days in MOF research[47] but must be used with care. As discussed by, e.g., Ling and Slater,[48] MOFs should be considered more as periodic arrays of self-assembled molecules with discrete molecular absorption modes as opposed to classical semiconductors. For clarity, we opt to use the classical band gap terminology in the remainder of this work.

The aim of the present contribution is to provide insight into the optical characteristics of substituted UiO-66-X frameworks (Scheme 1) using ab initio methods in direct comparison to

Scheme 1. Main Types of Linkers Studied in This Work: X = NH_2, OH, SH

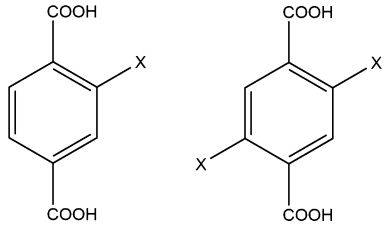

experimental measurements. Since we are concerned only with the absorption properties of the framework as such (without including, e.g., adsorbed guest molecules), we refer to "intrinsic" light-absorption properties in this work.

The accurate simulation of excited-state spectroscopic properties has progressed enormously in recent years. This can mainly be attributed to the success of time-dependent DFT (TD-DFT)[49,50] in its linear response formulation, which can be used to calculate excited states for systems of relatively large size at a feasible computational cost.[51] TD-DFT is particularly effective for the study of low-lying valence excited states of molecular systems.[52] Seminal work by Barone and co-workers has revealed that TD-DFT is able to provide accurate one-photon excitation and emission properties of organic molecular systems, even including vibrational coupling.[53] It has been reported that the main line shape of the electronic spectra is reasonably reproduced by the majority of modern DFT functionals, whereas the main difference between theory and experiment originates from the choice of the selected DFT functional.[54,55] Moreover, effects of the molecular environment and dynamic effects of the structure are essential when comparison with experiment is foreseen.[56] The dynamic effects are due to the inherent flexibility and vibrational motions of the molecule under investigation. It is now accepted that averaging over different configurations—generated during a molecular dynamics (MD) simulation—leads to reliable dynamic estimations of transition properties that are in good agreement with experimental data. Some of the present authors previously applied a dynamic approach to successfully characterize halochromic dyes[57] and carbonaceous compounds present as reaction intermediates in a zeolite-catalyzed process,[58] and on the basis of this success, dynamic averages are also presented in this work. The dynamic simulations provide insight into the key geometrical characteristics that are responsible for the changes

DOI: 10.1021/acs.inorgchem.5b01593
Inorg. Chem. XXXX, XXX, XXX−XXX

in transition positions and intensities. Moreover, a deeper understanding of the band gap modulation upon linker functionalization is obtained by comparing the experimental UV/vis spectra directly with the theoretical calculations on the fully periodic frameworks for a range of functionalizations. Because semilocal DFT functionals are known to underestimate the band gap,[59] we performed calculations with the hybrid HSE functional.[60−63] This functional has already been used to calculate the band gaps of UiO-66-NH_2 and UiO-66-NO_2 frameworks and showed excellent agreement with the experimental values.[44] Tuning of the absorption of UiO-66 frameworks and a clear understanding of the underlying electronic effects in the materials are important steps toward the development of molecular engineered catalysts.

2. MATERIALS AND METHODS

2.1. Experimental Details. *2.1.1. Materials.* All of the linkers except SH-functionalized H_2BDC are commercially available (Sigma-Aldrich, TCI) and were used without further purification. The H_2BDC-2,5SH linker was produced following a recipe by Vial et al.,[64] which is provided in section S1 in the Supporting Information (SI).

2.1.2. MOF Synthesis. UiO-66-X was synthesized following the general procedure described by Biswas and Van Der Voort[65] using commercial reagents. In a Pyrex tube, 0.31 mmol of $ZrOCl_2{\cdot}8H_2O$ was mixed with 0.31 mmol of the linker precursor (X-benzene-1,4-dicarboxylic acid (H_2BDC-X)), 1.2 mL of formic acid as a modulator, and 3 mL of *N*,*N*-dimethylacetamide (DMA) as the solvent. The resulting mixture was heated at 150 °C for 24 h, and the solid product was filtered off and washed several times with acetone. The resulting "as synthesized" material (UiO-66-AS) was stirred in *N*,*N*-dimethylformamide (DMF) for 12 h and then in methanol for 24 h to remove unreacted linker. Afterward, the sample was dried under vacuum at 65 °C for 24 h. For UiO-66-X samples with X ≠ H, further heating to 180 °C was necessary. Photographs of the final products are shown in section S2 in the SI.

2.1.3. Characterization. MOF materials were characterized by powder X-ray diffraction (PXRD) and N_2 absorption measurements. PXRD patterns for all of the MOF materials are provided in section S3 in the SI. Ambient-temperature PXRD patterns were recorded on a Thermo Scientific ARL XTra diffractometer operating at 40 kV and 40 mA using Cu Kα radiation (λ = 1.5406 Å). The sorption isotherms were measured on a Belsorp Mini apparatus at 77 K.

Solid-state UV/vis measurements were done on a Varian Cary 500 dual-beam UV/vis/near-IR spectrophotometer using an internal 110 mm $BaSO_4$-coated integrating sphere. Liquid experiments were carried out in solvent (DMF) on a PerkinElmer Lambda 900 UV/vis/NIR spectrometer. The spectrum of H_2BDC-2,5SH dissolved in DMF showed the appearance of an extra band. For a better comparison, the spectrum of this product was measured in methanol and showed only one clearly defined peak. Band gaps were extracted by extrapolating the cutoff wavelength to the *x*-intercept, similar to the procedure reported by Musho et al.[45]

2.2. Computational Details. *2.2.1. Geometry Generation and Excited-State Calculations on Linker and Cluster Models.* Static calculations on the linkers and clusters were done in Gaussian 09 (G09)[66] using DFT. Gas-phase linker models as shown in Scheme 1 were considered. We performed an initial assessment study of the influence of the basis set and DFT functional, which is summarized in section S4 in the SI. Our results pointed toward the B3LYP hybrid functional[67,68] in combination with a Pople 6-311+G(d,p) basis set[69] as appropriate for the study at hand. This level of theory was selected for both optimization of the structures and the TD-DFT calculations. This method was previously shown to provide reliable data on light absorption by organic structures of similar size.[70] Solvent effects (DMF) were included during TD-DFT calculations using a bulk solvent model, namely, the polarizable continuum model (ε = 37.219) within the integral equation formalism[71] as implemented in the G09 package.

The cluster models consisted of one metal node ($Zr_6O_4(OH)_4$) and two linkers (in the singly protonated form HBDC-X^-). The 10 remaining coordination sites were terminated by formate anions ($HCOO^-$). The resulting stoichiometry of the cluster model is given by $Zr_6O_4(OH)_4(HCOO)_{10}$(HBDC-X)$_2$. Since Zr atoms are not included in the Pople basis set, the cluster calculations were performed using the triple-ζ Def2TZVP basis set[72] and the same DFT functional. The clusters were optimized by retaining the metal node geometry as in the periodic structure and optimizing only the linker positions (resulting in a slight torsion depending on the functional group).

The optimized ground-state structures were employed to derive absorption data for the involved linkers and cluster models of the UiO-66 MOFs. Vertical transitions can be considered as an initial approximation for experimental UV/vis spectra and can provide clear insight into relative trends of the influence of linker substitution.[57] The computationally obtained transitions were broadened using a Gaussian distribution (eq 1) with a standard deviation of σ = 0.4 eV for comparison with the experimental spectra:

$$f(\nu) = f^{\max} \exp\left[-\left(\frac{\nu - \tilde{\nu}}{\sigma}\right)^2\right] \quad (1)$$

The percentages of orbital contributions were calculated by a Mulliken-type approach using the orbital coefficients and the overlap matrix as implemented in the Chemissian program.[73]

Charge calculations on the linker systems were done using the Horton program.[74] In this program, an iterative Hirshfeld scheme[75] is implemented, applying the classical Hirshfeld scheme in a self-consistent way. This method has been assessed extensively in the literature for different systems to test for sensitivity to the basis set and level of theory, dependence on the molecular geometry, etc.[76−78] This scheme has been successfully implemented for periodic systems[79,80] as a module in the HIVE version 3.x package, allowing comparison with the simulations on the fully periodic frameworks.[81]

In case of the linker models, dynamic averages of the absorption properties were obtained using ab initio molecular dynamics simulations. Snapshots were extracted from the generated trajectories, and TD-DFT simulations were performed on them using the theoretical methodology indicated above. Averaging over all of the resulting snapshots gives the final dynamic averages. All details of the MD-based data are included in section S5 in the SI.

2.2.2. Band Structure Calculations on the Fully Periodic Models. All of the periodic calculations were performed within the VASP package[82−84] using the PBE functional.[85] The plane-wave basis set had a kinetic energy cutoff of 500 eV, and a Γ-centered 3 × 3 × 3 **k**-point set was used to sample the first Brillouin zone. All of the structures were relaxed using a conjugate-gradient method with the energy convergence criterion set to 10^{-7} eV. As a result, the maximum force on an atom at the end of a relaxation was <1 meV/Å. During the structure optimization we constrained the cell volume to be equal to that of the pure UiO-66 MOF, taken from Valenzano and co-workers.[86] Only the cell shape and internal positions were optimized in order to reduce the computational cost, with the assumption that the band structure does not change significantly on a qualitative scale with volume optimization. The resulting structures retained their fcc nature with only small distortions of the lattice parameters (<0.1 Å) and lattice angles (<0.5°). The lattice parameters can be found in section S6 in the SI. All of the calculations were performed using the primitive fcc unit cell containing six Zr atoms (i.e., one Zr−O cluster) and six linkers. As such, the unit cell of the unfunctionalized UiO-66 material contained 114 atoms, which could increase to as many as 126 atoms depending on the functionalization. The PBE density of states (DOS) was obtained using a 5 × 5 × 5 **k**-point grid, and the PBE band structure was obtained along the high-symmetry lines Γ−X, Γ−L, and Γ−K. Since PBE is known to underestimate the band gap,[59] we performed computationally very expensive HSE06[60−63] calculations. The HSE06 DOS was obtained by performing a single static run starting from the PBE electron density. To make the calculations computationally feasible, the **k**-point set used for the HF exact-exchange part of the functional was reduced to the Γ point only, and

DOI: 10.1021/acs.inorgchem.5b01593
Inorg. Chem. XXXX, XXX, XXX−XXX

the remaining DFT contributions were calculated on a 3 × 3 × 3 **k**-point grid.

3. RESULTS AND DISCUSSION

3.1. Electronic Absorption Spectra of the Linkers.

3.1.1. Experimental Results. The main linkers studied in this work are schematically represented in Scheme 1. For NH_2 and OH functionalization, both the mono- and difunctionalized linkers are commercially available, while the SH linker was synthesized in our lab following a procedure provided in the SI. Taking H_2BDC as the reference, in which the carboxylic groups are at positions 1 and 4, the functionalizations are at position 2 or positions 2 and 5. Henceforth we denote the monofunctionalized H_2BDCs as H_2BDC-X and the difunctionalized H_2BDCs as H_2BDC-2,5X (X = NH_2, OH, SH). The investigated functional groups all exhibit electron-donating character.

Figure 2A shows the experimental absorption spectra of the DMF-solvated linkers H_2BDC, H_2BDC-NH_2, H_2BDC-2,5NH_2,

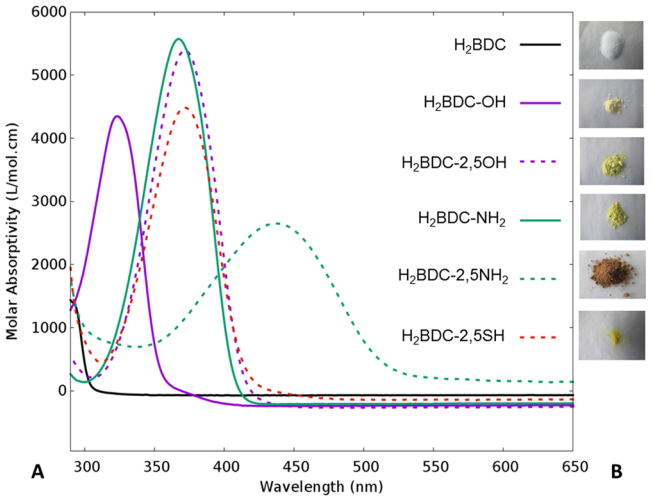

Figure 2. (A) Experimental linker spectra. (B) Photographs of the pure linkers.

H_2BDC-OH, H_2BDC-2,5OH, and methanol solvated H_2BDC-2,5SH. It can be observed that pristine H_2BDC shows no absorption in the visible region (also see section S7 in the SI), while clear absorption bands do appear for the H_2BDC-X linkers. The shift of the H_2BDC-OH linker remains modest (±32 nm), but for the other linkers, shifts of about 70−80 nm are observed, and H_2BDC-2,5NH_2 has a band shifted by 150 nm compared with the parent H_2BDC linker. The H_2BDC-SH material was not studied experimentally but is included in the theoretical calculations for comparison. Figure 2B clearly shows an intensifying color as the functionalization is changed, ranging from white to light yellow to dark yellow. The larger shift of the disubstituted linker in comparison with the monosubstitued variant is similar for all of the functional groups (about 50−70 nm). The interesting possibilities of these doubly functionalized linkers have been used by Sun et al.[41] to make a mixed UiO-66-NH_2/UiO-66-2,5NH_2 MOF featuring a larger activity in the photocatalytic reduction of CO_2.

3.1.2. Theoretical Absorption Spectra and Charge Analysis. To obtain further insight into the molecular origin of the absorption spectra, a variety of theoretical calculations were performed. In Figure 3, the static TD-DFT results for each separate linker are compared with the experimental spectra of the linker and the corresponding MOF. Herein, only the transitions to the first excited state are included, since the higher excitations are in the UV region. Figure 3 demonstrates the ability of static TD-DFT calculations to predict the experimental absorption bands of the isolated linkers with high accuracy. Both the excitation wavelength and oscillator strength are computed with good accuracy compared with experiment. The computed oscillator strength f is coupled to the experimental molar absorptivity ε as follows:

$$f_{i,\max} \sim \tilde{\nu} \cdot D_{i,\max}$$

$$D_{i,\max} \sim \varepsilon_i^{\max} \cdot \frac{1}{\tilde{\nu}} \qquad (2)$$

These general equations show that the dimensionless oscillator strength at the maximum of the absorption ($f_{i,\max}$) is proportional at a certain energy to the frequency ($\tilde{\nu}$) and the dipole strength D, which in turn can be linked to the molar absorptivity ε. In this work, we will consistently use these equations in order to make direct comparisons of calculated and experimental intensities.

Analysis of the orbitals involved in the excitation indicates that the HOMO−LUMO excitation is the dominant contribution. The corresponding orbitals are incorporated in Figure 3, and they show that the contribution of the functional groups almost vanishes in the LUMOs. For example, the functional group in the case of the H_2BDC-NH_2 linker constitutes up to 39% of the HOMO, whereas this is reduced to only 2% in the LUMO. Since the first excited state is mainly composed of this LUMO, the functional groups have almost no contribution in this state.

In order to further quantify this effect, we performed Hirshfeld charge calculations based on the ground-state and excited-state electron densities. The most important results are shown in Table 1, and the complete calculation set can be found in section S8 in the SI. For the monofunctionalized linkers, we find a large charge shift in the ring system, with the order OH < NH_2 < SH. This order is consistent with the drop in electronegativity[87] (EN(O) > EN(N) > EN(S)). The same trend is found for the doubly functionalized linker. However, since electron-donating subtituents have a para-directing influence on the electronic structure of the aromatic system, there is a small counteracting influence, and hence, the contribution per substituent is smaller.

The influence of temperature on the theoretical spectra was assessed by sampling of the ground-state potential energy surface using MD simulations and subsequent calculation of dynamic averages of the excitation properties.[57] The resulting dynamic averages for all of the studied linkers, together with the experimental and theoretical static values, are included in Table S2 in the SI. The dynamic averages of the predicted absorption maxima are found to be larger than their static counterparts (the shifts range between 0 and 31 nm) as a result of the inclusion of temperature effects. The H_2BDC-2,5OH linker is the only exception, exhibiting a dynamic λ value that is 3 nm smaller than the statically obtained result. It must also be stressed that the level of theory employed for the generation of the geometries differs in case of the static and dynamic values. Notably, the MD-based approach does not automatically improve the agreement with the experimental values. Hence, in-depth research using more advanced tools[88] is necessary to

DOI: 10.1021/acs.inorgchem.5b01593
Inorg. Chem. XXXX, XXX, XXX−XXX

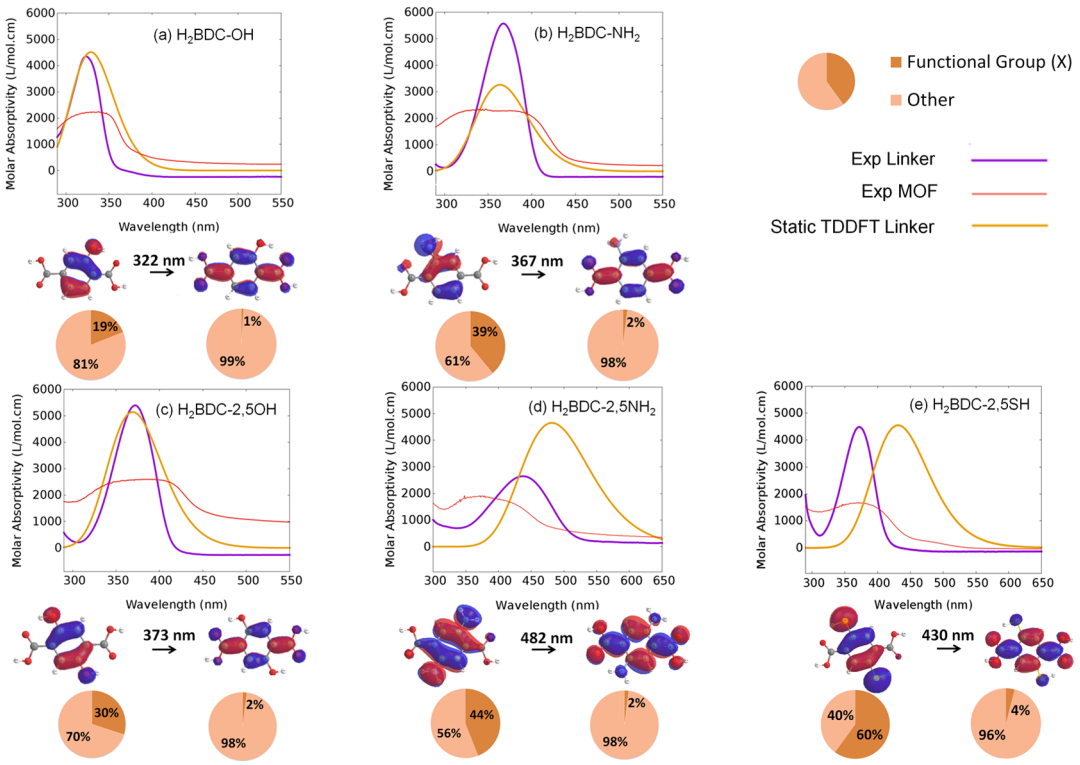

Figure 3. Plots of the experimental UV/vis spectra (purple lines) and the TD-DFT (B3LYP/6-311+G(d,p)) calculated spectra (only the first excitations are plotted, orange lines) of the isolated linkers. The experimental diffuse-reflectance spectra of the MOFs (red lines) are also shown, and their intensities have been arbitrarily scaled for comparison. The orbitals of the ground and excited states (HOMO and LUMO, respectively) are depicted, and the contributions of the functional group vs the ring system are provided in the pie plots, showing the shift in orbital contribution toward the aromatic ring system. Monosubstituted (a, b) and disubstituted (c–e) structures are shown. For the 2,5X structures (c–e), the cumulative effect of the two functional groups is reported.

Table 1. Iterative Hirshfeld Charges of the Substituents Obtained for the Ground State (GS) and Excited State (ES) Densities Using B3LYP/6-311+G(d,p) and a PCM Solvent Model

X	GS charge	ES charge	Δ
	H_2BDC-X		
NH_2	−0.14(3)	0.15(9)	0.30
OH	−0.17(4)	−0.02(9)	0.14
SH	0.03(8)	0.96(9)	0.93
	H_2BDC-2,5X		
NH_2	−0.14(0)	0.03(3)	0.17
OH	−0.18(7)	−0.06(9)	0.12
SH	0.03(3)	0.26(1)	0.23

fully unravel why some functionalized linkers are more affected by dynamic features than others.

In conclusion, the following general observations can be made on the basis of the analysis of the theoretical calculations on the organic linker models. The different functionalities have an increasing electron-donating effect on the aromatic ring, shifting the absorption maximum in the following order: H < OH < NH_2 < SH. Static calculations accurately predict the peak positions and intensities of the OH-functionalized linkers, but for the other systems, it is suggested that dynamic effects should be taken into account. The TD-DFT-based method yields accurate results, and the experimental values are reproduced well. For the NH_2 linkers, in particular the difunctionalized variant, the calculated values overestimate the experimental absorption maxima.

3.2. Electronic Absorption Spectra of Inorganic–Organic Cluster Models. In the literature, it has been suggested that the photocatalytic activity of the UiO-66 materials can be attributed to a ligand-to-metal charge transfer (LMCT) process.[41] The authors performed photoluminescence measurements and hence provided experimental data to confirm this hypothesis. In this process, light is absorbed via the (NH_2-)functionalized linker, after which energy transfer toward the inorganic nodes takes place. In this way, the absorbed energy can be used to initiate redox reactions at these reactive sites. In order to investigate possible LMCT effects theoretically, inorganic–organic clusters based on the periodic structures were constructed. This procedure was previously followed by some of the presenting authors to study reactivity in UiO-66 materials.[23]

Figure 4 shows the HOMO, LUMO, and LUMO+1 in the case of the BDC-2,5OH linker (which is present in the singly protonated form HBDC-2,5OH^- in the cluster model). As was the case with the linker studies (Figure 3), the HOMO and LUMO are found to play the major role in the visible-light excitation, considering both the oscillator strength f and the wavelength λ. Hence, the peak positions of these calculations yield the same trends as found with the linker calculations (cf. section S9 in the SI). A similar static analysis of the orbital contributions as for the bare linkers was performed as well. This shows that the HOMOs are localized on the linkers and that exciting the system at 369 nm causes a shift of about 18% of the orbital contributions to the inorganic cluster (see Figure 4). If we look at the excitation involving the HOMO to LUMO+1 transition (at 298 nm in the case of BDC-2,5OH; see Figure 4),

DOI: 10.1021/acs.inorgchem.5b01593
Inorg. Chem. XXXX, XXX, XXX–XXX

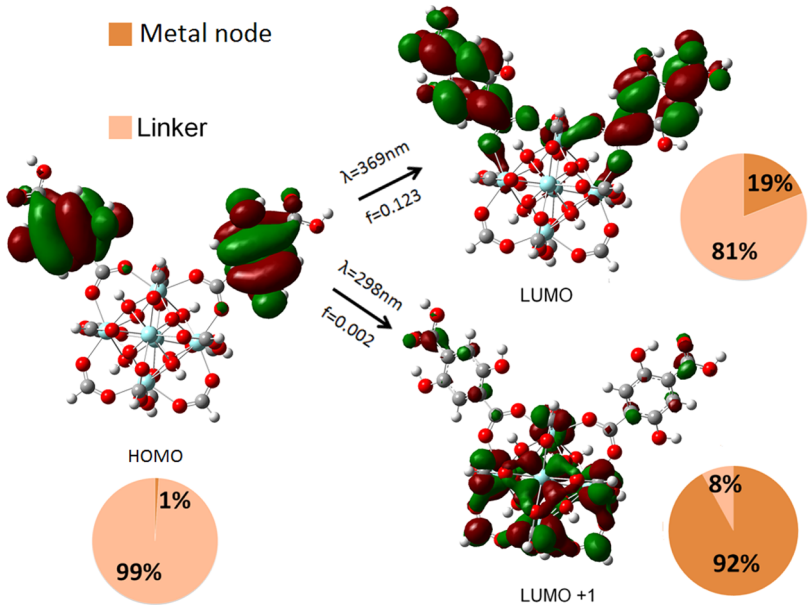

Figure 4. Scheme representing the first and second excitations for the cluster model with BDC-2,5OH linkers (having the stoichiometry $Zr_6O_4(OH)_4(HCOO)_{10}(HBDC\text{-}2,5OH)_2$). TD-DFT calculations were performed at the B3LYP/Def2TZVP level of theory.

the contribution of the linkers almost completely disappears, resulting theoretically in a large shift of the orbital contributions toward the inorganic metal nodes. However, the calculated oscillator strength of this excitation is almost zero, and hence, it makes almost no contribution in the total excitation spectrum. These theoretical results indicate that LMCT occurs to only a limited extent in these systems upon visible-light radiation. If we look for example at the BDC-OH linker in this cluster, the same general behavior can be observed, but the first excitation has an orbital shift of only 10% instead of the 18% observed in the doubly functionalized system.

Figure 5 summarizes the transfers of orbital contributions in the first excitation (HOMO to LUMO) for all of the

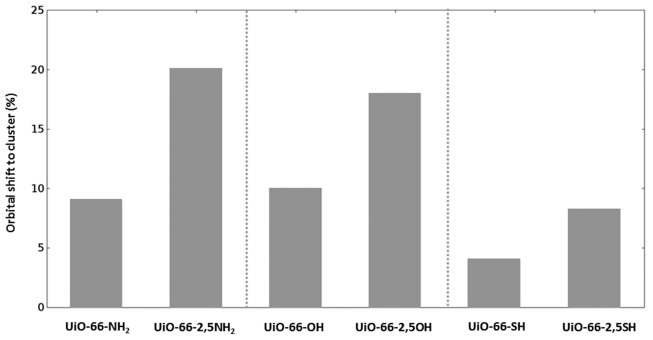

Figure 5. LMCT in the first excitation (HOMO to LUMO) for each of the MOFs, representing the transfer of orbital contributions from the organic linker to the inorganic metal node. The calculations were done on the corresponding cluster models as shown in Figure 4.

inorganic−organic clusters. These data represent the LMCT from the organic linker to the inorganic Zr−O node upon excitation expressed in terms of the shift in orbital contribution. As a general trend, we observe that multiple substitution has an extra electron-donating influence in these cluster models. This effect can explain the higher catalytic activity as observed by Sun et al.[41] The use of doubly functionalized linkers or a mixed-linker approach can hence be beneficial when developing a new photocatalyst.

3.3. Electronic Properties of the Fully Periodic UiO-66 Frameworks. In this third part, the experimental and theoretical results for the periodic UiO-66 materials are discussed in detail and related to the observed linker results.

Organic linkers embedded in MOFs, by their very nature, are expected to be quite comparable to their free molecular counterparts. Although the lattice introduces some constraints on their geometry, their electronic structure is expected to be more or less unaltered apart from possible charge transfer effects as discussed in the previous section. Comparison of the embedded linkers and the free molecular linkers indicates that the geometry of the functional groups is retained even after structure optimization in the periodic systems (see section S10 in the SI). Moreover, the calculated Hirshfeld-I charges show that despite the variation in type and number of functional groups, the total linker charges as well as the charges of the Zr atoms barely vary among the different functionalized UiO materials, as was also observed for functionalized MIL-47.[89] This means that without excitation of the electronic structure, the different functionalizations of the linkers do not influence the electronic structure of the ZrO clusters. To obtain a more detailed understanding of the electronic structure of the functionalized UiO-66 materials, their densities of states (DOS) and band structures are investigated below.

3.3.1. Experimental UV/Vis Spectra and Theoretical Band Gaps of the UiO-66-X Frameworks. The experimental UV/vis spectra shown in Figure 3 indicate that the pure linker peaks overlap with the absorption maxima of the corresponding UiO-66-X materials. On the other hand, the spectra of the periodic materials show significant broadening. This immediately becomes clear when we compare the pure linker powders with the frameworks, as shown in section S2 in the SI. The color variations indicate that the electronic band structure around the band gap is significantly modified.

This is indeed supported by the periodic simulations of the UiO-66-X materials. In all cases, a direct band gap was found. As an example, Figure 6 shows the band structure and DOS of

DOI: 10.1021/acs.inorgchem.5b01593
Inorg. Chem. XXXX, XXX, XXX−XXX

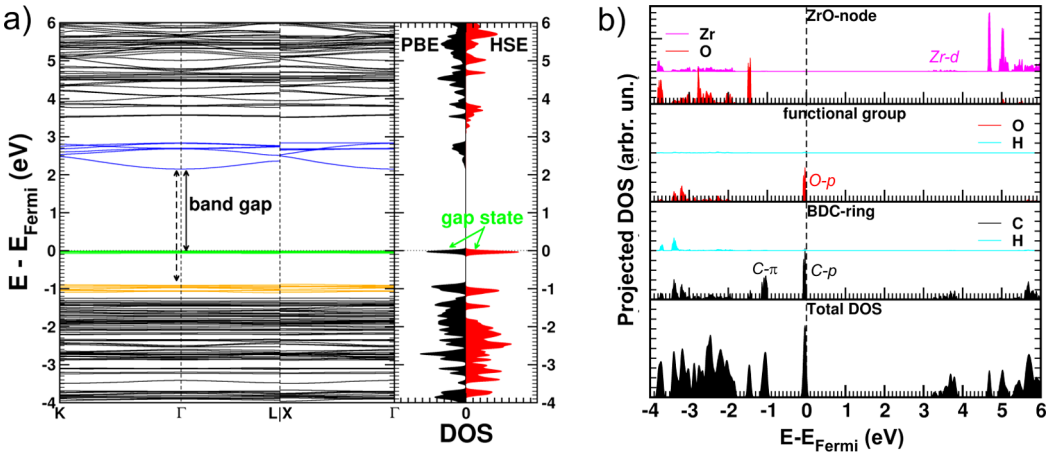

Figure 6. Calculated electronic properties of UiO-66-OH. (a) Band structure and DOS. The band structure was obtained using the PBE functional, while the DOS was obtained using both the PBE and HSE06 functionals. The band gap is depicted as a solid arrow, while the energy difference relating to the band gap of the unfunctionalized UiO-66 material is represented as a dotted arrow. (b) Total DOS obtained using the HSE06 functional (black curve). The site-projected DOS of relevant atoms are indicated as offset curves and grouped according to the Zr−O node (Zr, pink; O, red), functional group (O, red; H, cyan) and BDC ring (C, black; H, cyan).

UiO-66-OH. Comparison of the PBE and HSE06 DOS shows them to present the same qualitative picture, while quantitatively the main difference is the larger band gap for the HSE06 DOS. The calculated band gaps for the different functionalized UiO-66 MOFs are compared to our experimentally determined values in Figure 7. All of the calculated

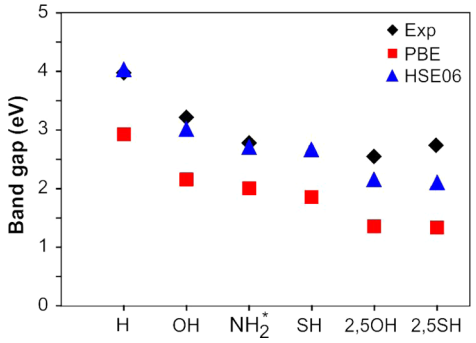

Figure 7. Band gaps for various functionalized UiO-66 materials. The theoretical values for NH_2 were taken from ref 44.

data are reported in section S11 in the SI. It is clear that although the PBE values significantly underestimate the experimental band gaps, they do represent the experimentally observed trends. The HSE06 band gaps, on the other hand, also show good quantitative agreement with experiment. These accurate data indicate that linker functionalization can lead to band gaps ranging between 4.0 and 2.2 eV and that engineering of the band gap of the UiO-66 materials is possible.

3.3.2. Density of States and Band Structure Analysis. Careful comparison of the different densities of states shows that the electronic structures of the functionalized and unfunctionalized UiO-66 frameworks are quite similar. However, contrary to the unfunctionalized material, UiO-66-X materials possess a filled band within the original band gap, a so-called gap state. This therefore corresponds to the new valence band, lowering the effective band gap substantially. In contrast, the energy difference corresponding to the band gap of the host material remains roughly constant for all of the functional groups (3.0 eV for PBE and 4.0 eV for HSE06; cf. section S10 in the SI). In the case of the doubly functionalized UiO-66-2,5SH material, a second band can also be identified just above the valence band of the host material (cf. section S10). This is not the case for the PBE DOS of UiO-66-2,5OH, although the HSE06 DOS indicates that this band might overlap with the top of the valence band. We will not discuss this band further, as it does not influence the spectroscopic properties of UiO-66-X.

Projected densities of states (PDOS) provide more insight into the origins of distinct bands by projecting the corresponding orbitals on the different atoms. This is illustrated in Figure 6b for the UiO-66-OH material, but similar conclusions are valid for the other functionalized UiO-66 materials. The electron densities of these bands are plotted in section S12 in the SI. We find that the gap state has a recognizable fingerprint for each UiO-66-X: it is mainly of p character associated with the C atoms of the ring and the S/O atom of the functional group(s). This indicates that the functional group forms a bond with the π orbitals of the aromatic ring. Importantly, the occupation remains the same: two electrons per functional group in the system, indicative of the bond between the functional group and the ring. The width of the functionalization-induced band depends on the employed functional and the type of functional group but not on the number of functional groups on the linker (cf. Table S8 in the SI). The π orbitals of the linker ring themselves give rise to the top levels of the valence band. In contrast, the conduction band is rather insensitive to the functional group: the conduction band character mainly corresponds to that of the Zr d electrons or to orbitals delocalized over the entire linker.

We conclude that the band gap of the host material remains largely the same, but upon functionalization, the π orbital splits into two bands (cf. section S10 in the SI). One of these bands remains in position, while the other band, which contains contributions from the functional group, moves upward, giving rise to a fully filled gap state and a reduced effective band gap. As a consequence, excitation of the linker electrons from this newly split-off gap state is much easier, which explains the decreasing trend in the band gap upon functionalization (see Figure 7).

DOI: 10.1021/acs.inorgchem.5b01593
Inorg. Chem. XXXX, XXX, XXX−XXX

4. CONCLUSIONS

The optical absorption properties of functionalized Zr(UiO-66)-type metal−organic frameworks were investigated using experimental UV/vis measurements combined with theoretical simulations. The benzene-1,4-dicarboxylic acid linker unit was mono- or bifunctionalized with various electron-donating substituents, i.e., OH, NH_2, and SH, and the resulting effect on the absorption properties was examined. The effect of the nanoporous framework was directly assessed via simulations of the solvated linkers, extended clusters, and fully periodic materials.

Theoretical absorption spectra of the various functionalized linkers were obtained using time-dependent density functional theory with the B3LYP hybrid functional. Vertical transition energies of the substituted linkers already provided a good agreement with experiment, in particular for the OH-substituted linkers. The correct trend was obtained for the monofunctionalized cases, meaning that the absorption maximum increases in going from OH to NH_2 to SH. Interpretation of the orbitals involved in the main transition clearly pointed toward charge transfer from the functional group to the aromatic ring of the linker molecule.

For all of the linkers, the static data were compared with dynamic averages obtained from ab initio molecular dynamics simulations and subsequent TD-DFT simulations on extracted snapshots. These dynamic averages were found to be larger than the static values, although no systematic change was found for the whole test set. To investigate the precise origin of the observed shifts, future work will be performed with dedicated analysis tools.

In the next phase, inorganic−organic clusters were considered in order to examine the amount of charge transfer between the organic linkers and the metal nodes. Static TD-DFT simulations on an extended cluster model indicated that the corresponding first excitation is found at almost the same wavelength as for the linker situation. In this transition, there is a small transfer of orbital contribution to the metal nodes, but the LUMO orbital involved in the excitation is still mainly located on the linker units. The amount of transfer is functionalization-dependent and was shown to be the largest in the case of BDC-2,5NH_2.

Fully periodic models were also employed to corroborate our findings. In addition to PBE, the hybrid HSE06 functional was used to investigate the electronic structure of the functionalized Zr(UiO-66)-type metal−organic frameworks. The existence of a gap state within the band gap of the unfunctionalized UiO-66 was shown to be the reason for the observed band gap modulation. The HSE06 calculations on the fully periodic models provided band gaps in excellent agreement with the experimental values. The band gaps ranged between 4.0 and 2.2 eV, indicating that linker functionalization is indeed an excellent procedure to modify the band gap of the metal−organic framework. The simulations suggest that materials containing the same type of linkers should show similar behavior. However, we believe that more research is warranted to investigate whether MOF materials with the same organic linkers but varying inorganic units would give similar absorption properties.

■ ASSOCIATED CONTENT

Supporting Information

The Supporting Information is available free of charge on the ACS Publications website at DOI: 10.1021/acs.inorgchem.5b01593.

H_2BDC-SH recipe, experimental powders, experimental XRD spectra, basis set test on the isolated H_2BDC-2,5OH linker, ab initio MD simulations of linker models, lattice parameters, UV/vis spectra of H_2BDC and UiO-66, charges of the isolated linkers, computated UV/vis absorption values of the cluster models, comparison of the geometries and charges of free and framework linkers, and a summary of the electronic properties of the periodic simulations (PDF)

■ AUTHOR INFORMATION

Corresponding Authors

*E-mail: Veronique.VanSpeybroeck@ugent.be.
*E-mail: Pascal.VanDerVoort@ugent.be.
*E-mail: Karen.Hemelsoet@UGent.be.

Present Address

[§]ArcelorMittal Gent, John Kennedylaan 51, 9042 Ghent, Belgium

Notes

The authors declare no competing financial interest.

■ ACKNOWLEDGMENTS

The Foundation for Scientific Research-Flanders (FWO), the Research Board of Ghent University (BOF, UGent GOA Grant 01G00710), and the European Research Council (FP7(2007-2013) Grant Agreement 240483) are acknowledged for their financial support. D.E.P.V. is a postdoctoral researcher funded by the FWO (Project 12S3415N). Computational resources and services were provided by the Stevin Supercomputer Infrastructure of Ghent University and by the Flemish Supercomputer Center (VSC), funded by the Hercules Foundation and the Flemish Government—Department EWI. Prof. Dr. D. Poelman is acknowledged for help with the UV/vis measurements.

■ REFERENCES

(1) Thematic issue on metal−organic frameworks: *Chem. Rev.* **2012**, *112*, 673−1268.
(2) Corma, A.; García, H.; Llabrés i Xamena, F. X. *Chem. Rev.* **2010**, *110*, 4606−4655.
(3) Liu, D.; Lu, K.; Poon, C.; Lin, W. *Inorg. Chem.* **2014**, *53*, 1916−1924.
(4) Wang, J.; Wang, C.; Lin, W. *ACS Catal.* **2012**, *2*, 2630−2640.
(5) Nasalevich, M. A.; van der Veen, M.; Kapteijn, F.; Gascon, J. *CrystEngComm* **2014**, *16*, 4919−4926.
(6) Allendorf, M. D.; Bauer, C. A.; Bhakta, R. K.; Houk, R. J. T. *Chem. Soc. Rev.* **2009**, *38*, 1330−1352.
(7) Cui, Y.; Chen, B.; Qian, G. *Struct. Bonding* **2013**, *157*, 27−88.
(8) Farrusseng, D. *Metal-Organic Frameworks: Applications from Catalysis to Gas Storage*; Wiley-VCH: Weinheim, Germany, 2011.
(9) Sun, C.; Wang, X.; Zhang, X.; Qin, C.; Li, P.; Su, Z.; Zhu, D.; Shan, G.; Shao, K.; Wu, H.; Li, J. *Nat. Commun.* **2013**, *4*, 2717.
(10) Hu, Z.; Deibert, B. J.; Li, J. *Chem. Soc. Rev.* **2014**, *43*, 5815−5840.
(11) Fujishima, A.; Honda, K. *Nature* **1972**, *238*, 37−38.
(12) Schneider, J.; Matsuoka, M.; Takeuchi, M.; Zhang, J.; Horiuchi, Y.; Anpo, M.; Bahnemann, D. W. *Chem. Rev.* **2014**, *114*, 9919−9986.

DOI: 10.1021/acs.inorgchem.5b01593
Inorg. Chem. XXXX, XXX, XXX−XXX

(13) van Dijken, A.; Janssen, A. H.; Smitsmans, M. H. P.; Vanmaekelbergh, D.; Meijerink, A. *Chem. Mater.* **1998**, *10*, 3513−3522.
(14) Hoffmann, M. R.; Martin, S. T.; Choi, W.; Bahnemann, D. W. *Chem. Rev.* **1995**, *95*, 69−96.
(15) Fox, M. A.; Dulay, M. T. *Chem. Rev.* **1993**, *93*, 341−357.
(16) Mills, A.; Le Hunte, S. *J. Photochem. Photobiol., A* **1997**, *108*, 1−35.
(17) Wang, Z. *Chin. Sci. Bull.* **2009**, *54*, 4021−4034.
(18) Linsebigler, A. L.; Lu, G.; Yates, J. T. *Chem. Rev.* **1995**, *95*, 735−758.
(19) Chowdhury, P.; Gomaa, H.; Ray, A. K. *ACS Symp. Ser.* **2013**, *1124*, 231−266.
(20) Kudo, A.; Miseki, Y. *Chem. Soc. Rev.* **2009**, *38*, 253−278.
(21) Zou, Z.; Ye, J.; Sayama, K.; Arakawa, H. *Nature* **2001**, *414*, 625−627.
(22) Beydoun, D.; Amal, R.; Low, G.; McEvoy, S. *J. Nanopart. Res.* **1999**, *1*, 439−458.
(23) Vermoortele, F.; Vandichel, M.; Van de Voorde, B.; Ameloot, R.; Waroquier, M.; Van Speybroeck, V.; De Vos, D. E. *Angew. Chem., Int. Ed.* **2012**, *51*, 4887−4890.
(24) Vermoortele, F.; Bueken, B.; Le Bars, G.; Van de Voorde, B.; Vandichel, M.; Houthoofd, K.; Vimont, A.; Daturi, M.; Waroquier, M.; Van Speybroeck, V.; Kirschhock, C.; De Vos, D. E. *J. Am. Chem. Soc.* **2013**, *135*, 11465−11468.
(25) Wu, P.; He, C.; Wang, J.; Peng, X.; Li, X.; An, Y.; Duan, C. *J. Am. Chem. Soc.* **2012**, *134*, 14991−14999.
(26) Fu, Y.; Sun, D.; Chen, Y.; Huang, R.; Ding, Z.; Fu, X.; Li, Z. *Angew. Chem., Int. Ed.* **2012**, *51*, 3364−3367.
(27) Horiuchi, Y.; Toyao, T.; Saito, M.; Mochizuki, K.; Iwata, M.; Higashimura, H.; Anpo, M.; Matsuoka, M. *J. Phys. Chem. C* **2012**, *116*, 20848−20853.
(28) Sun, D.; Ye, L.; Li, Z. *Appl. Catal., B* **2015**, *164*, 428−432.
(29) Wang, D.; Li, Z. *Catal. Sci. Technol.* **2015**, *5*, 1623−1628.
(30) Wang, D.; Huang, R.; Liu, W.; Sun, D.; Li, Z. *ACS Catal.* **2014**, *4*, 4254−4260.
(31) Cavka, J. H.; Jakobsen, S.; Olsbye, U.; Guillou, N.; Lamberti, C.; Bordiga, S.; Lillerud, K. P. *J. Am. Chem. Soc.* **2008**, *130*, 13850−13851.
(32) Wiersum, A.; Soubeyrand-Lenoir, E.; Yang, Q.; Moulin, B.; Guillerm, V.; Yahia, M.; Bourrelly, S.; Vimont, A.; Miller, S.; Vagner, C.; Daturi, M.; Clet, G.; Serre, C.; Maurin, G.; Llewellyn, P. *Chem. - Asian J.* **2011**, *6*, 3270−3280.
(33) Vandichel, M.; Hajek, J.; Vermoortele, F.; Waroquier, M.; De Vos, D.; Van Speybroeck, V. *CrystEngComm* **2015**, *17*, 395−406.
(34) Zhao, W.; Zhang, C.; Yan, Z.; Bai, L.; Wang, X.; Huang, H.; Zhou, Y.; Xie, Y.; Li, F.; Li, J. *J. Chromatogr. A* **2014**, *1370*, 121−128.
(35) Stassen, I.; Styles, M.; Van Assche, T.; Campagnol, N.; Fransaer, J.; Denayer, J.; Tan, J.; Falcaro, P.; De Vos, D.; Ameloot, R. *Chem. Mater.* **2015**, *27*, 1801−1807.
(36) Kim, S.; Lee, Y.; Hong, S.; Jang, M.; Ahn, W. *Catal. Today* **2015**, *245*, 54−60.
(37) Shen, L.; Wu, W.; Liang, R.; Lin, R.; Wu, L. *Nanoscale* **2013**, *5*, 9374−9382.
(38) Gomes Silva, C.; Luz, I.; Llabrés i Xamena, F. X.; Corma, A.; García, H. *Chem. - Eur. J.* **2010**, *16*, 11133−11138.
(39) Shen, L.; Liang, S.; Wu, W.; Liang, R.; Wu, L. *Dalton Trans.* **2013**, *42*, 13649−13658.
(40) Long, J.; Wang, S.; Ding, Z.; Wang, S.; Zhou, Y.; Huang, L.; Wang, X. *Chem. Commun.* **2012**, *48*, 11656−11658.
(41) Sun, D.; Fu, Y.; Liu, W.; Ye, L.; Wang, D.; Yang, L.; Fu, X.; Li, Z. *Chem. - Eur. J.* **2013**, *19*, 14279−14285.
(42) Shen, L.; Liang, R.; Luo, M.; Jing, F.; Wu, L. *Phys. Chem. Chem. Phys.* **2015**, *17*, 117−121.
(43) Goh, T.; Xiao, C.; Maligal-Ganesh, R. V.; Li, X.; Huang, W. *Chem. Eng. Sci.* **2015**, *124*, 45−51.
(44) Flage-Larsen, E.; Røyset, A.; Cavka, J. H.; Thorshaug, K. *J. Phys. Chem. C* **2013**, *117*, 20610−20616.
(45) Musho, T.; Li, J.; Wu, N. *Phys. Chem. Chem. Phys.* **2014**, *16*, 23646−23653.
(46) Hendon, C.; Tiana, D.; Fontecave, M.; Sanchez, C.; D'arras, L.; Sassoye, C.; Rozes, L.; Mellot-Draznieks, C.; Walsh, A. *J. Am. Chem. Soc.* **2013**, *135*, 10942−10945.
(47) Odoh, S. O.; Cramer, C. J.; Truhlar, D. G.; Gagliardi, L. *Chem. Rev.* **2015**, *115*, 6051−6111.
(48) Ling, S.; Slater, B. *J. Phys. Chem. C* **2015**, *119*, 16667−16677.
(49) Runge, E.; Gross, E. *Phys. Rev. Lett.* **1984**, *52*, 997−1001.
(50) *Time-Dependent Density Functional Theory*; Marques, M. A. L., Ullrich, C., Nogueira, F., Rubio, A., Burke, K., Gross, E. K. U., Eds.; Springer: Berlin, 2006.
(51) Adamo, C.; Jacquemin, D. *Chem. Soc. Rev.* **2013**, *42*, 845−856.
(52) Dreuw, A.; Head-Gordon, M. *Chem. Rev.* **2005**, *105*, 4009−4037.
(53) Bloino, J.; Biczysko, M.; Santoro, F.; Barone, V. *J. Chem. Theory Comput.* **2010**, *6*, 1256−1274.
(54) Barone, V.; Biczysko, M.; Bloino, J.; Carta, L.; Pedone, A. *Comput. Theor. Chem.* **2014**, *1037*, 35−48.
(55) Laurent, A. D.; Adamo, C.; Jacquemin, D. *Phys. Chem. Chem. Phys.* **2014**, *16*, 14334−14356.
(56) Pedone, A.; Prampolini, G.; Monti, S.; Barone, V. *Chem. Mater.* **2011**, *23*, 5016−5023.
(57) De Meyer, T.; Hemelsoet, K.; Van der Schueren, L.; Pauwels, E.; De Clerck, K.; Van Speybroeck, V. *Chem. - Eur. J.* **2012**, *18*, 8120−8129.
(58) Hemelsoet, K.; Qian, Q.; De Meyer, T.; De Wispelaere, K.; De Sterck, B.; Weckhuysen, B. M.; Waroquier, M.; Van Speybroeck, V. *Chem. - Eur. J.* **2013**, *19*, 16595−16606.
(59) Perdew, J. P. *Int. J. Quantum Chem.* **1985**, *28*, 497−523.
(60) Heyd, J.; Scuseria, G. E.; Ernzerhof, M. *J. Chem. Phys.* **2003**, *118*, 8207−8215.
(61) Heyd, J.; Peralta, J. E.; Scuseria, G. E.; Martin, R. L. *J. Chem. Phys.* **2005**, *123*, 174101.
(62) Heyd, J.; Scuseria, G. E.; Ernzerhof, M. *J. Chem. Phys.* **2006**, *124*, 219906.
(63) Brothers, E. N.; Izmaylov, A. F.; Normand, J. O.; Barone, V.; Scuseria, G. E. *J. Chem. Phys.* **2008**, *129*, 011102.
(64) Vial, L.; Ludlow, R. F.; Leclaire, J.; Pérez-Fernández, R.; Otto, S. *J. Am. Chem. Soc.* **2006**, *128*, 10253−10257.
(65) Biswas, S.; Van Der Voort, P. *Eur. J. Inorg. Chem.* **2013**, *2013*, 2154−2160.
(66) Frisch, M. J.; et al. *Gaussian 09*, revision D.01; Gaussian, Inc.: Wallingford, CT, 2009.
(67) Lee, C.; Yang, W.; Parr, R. G. *Phys. Rev. B: Condens. Matter Mater. Phys.* **1988**, *37*, 785−789.
(68) Becke, A. D. *J. Chem. Phys.* **1993**, *98*, 5648−5652.
(69) Krishnan, R.; Binkley, J.; Seeger, R.; Pople, J. *J. Chem. Phys.* **1980**, *72*, 650−654.
(70) Jacquemin, D.; Perpète, E.; Scuseria, G.; Ciofini, I.; Adamo, C. *J. Chem. Theory Comput.* **2008**, *4*, 123−135.
(71) Tomasi, J.; Mennucci, B.; Cammi, R. *Chem. Rev.* **2005**, *105*, 2999−3093.
(72) Weigend, F.; Ahlrichs, R. *Phys. Chem. Chem. Phys.* **2005**, *7*, 3297−3305.
(73) http://www.chemissian.com.
(74) Verstraelen, T. *Horton*, 2011; available at http://theochem.github.com/horton/.
(75) Bultinck, P.; Van Alsenoy, C.; Ayers, P. W.; Carbó-Dorca, R. *J. Chem. Phys.* **2007**, *126*, 144111.
(76) Bultinck, P.; Ayers, P. W.; Fias, S.; Tiels, K.; Van Alsenoy, C. *Chem. Phys. Lett.* **2007**, *444*, 205−208.
(77) Verstraelen, T.; Ayers, P. W.; Van Speybroeck, V.; Waroquier, M. *Chem. Phys. Lett.* **2012**, *545*, 138−143.
(78) Verstraelen, T.; Pauwels, E.; De Proft, F.; Van Speybroeck, V.; Geerlings, P.; Waroquier, M. *J. Chem. Theory Comput.* **2012**, *8*, 661−676.
(79) Vanpoucke, D. E. P.; Bultinck, P.; Van Driessche, I. *J. Comput. Chem.* **2013**, *34*, 405−417.
(80) Vanpoucke, D. E. P.; Van Driessche, I.; Bultinck, P. *J. Comput. Chem.* **2013**, *34*, 422−427.

DOI: 10.1021/acs.inorgchem.5b01593
Inorg. Chem. XXXX, XXX, XXX−XXX

(81) Vanpoucke, D. E. P. *HIVE*, version 3.x., 2011; available at http://dannyvanpoucke.be/.
(82) Kresse, G.; Furthmüller, J. *Comput. Mater. Sci.* **1996**, *6*, 15−50.
(83) Hafner, J. *J. Comput. Chem.* **2008**, *29*, 2044−2078.
(84) Kresse, G.; Joubert, D. *Phys. Rev. B: Condens. Matter Mater. Phys.* **1999**, *59*, 1758−1775.
(85) Perdew, J. P.; Burke, K.; Ernzerhof, M. *Phys. Rev. Lett.* **1996**, *77*, 3865−3868.
(86) Valenzano, L.; Civalleri, B.; Chavan, S.; Bordiga, S.; Nilsen, M. H.; Jakobsen, S.; Lillerud, K. P.; Lamberti, C. *Chem. Mater.* **2011**, *23*, 1700−1718.
(87) Pauling, L. *J. Am. Chem. Soc.* **1932**, *54*, 3570−3582.
(88) Van Yperen-De Deyne, A.; De Meyer, T.; Pauwels, E.; Ghysels, A.; De Clerck, K.; Waroquier, M.; Van Speybroeck, V.; Hemelsoet, K. *J. Chem. Phys.* **2014**, *140*, 134105.
(89) Biswas, S.; Vanpoucke, D. E. P.; Verstraelen, T.; Vandichel, M.; Couck, S.; Leus, K.; Liu, Y.-Y.; Waroquier, M.; Van Speybroeck, V.; Denayer, J. F. M.; Van Der Voort, P. *J. Phys. Chem. C* **2013**, *117*, 22784−22796.

DOI: 10.1021/acs.inorgchem.5b01593
Inorg. Chem. XXXX, XXX, XXX−XXX